Polarization Dependent Raman Active Modes Study of the $Mo_{1-x}W_xS_2$ Mixed Layered Crystals

Dumitru O. Dumcenco,[1] Yu-Chen Su,[1] Yi-Ping Wang,[1] Kuei-Yu Chen,[1] Ying-Sheng Huang,[1,*] Ching-Hwa Ho,[1] and Kwong-Kau Tiong[2]

[1] *Department of Electronic Engineering, National Taiwan University of Science and Technology, Taipei 106, Taiwan*

[2] *Department of Electrical Engineering, National Taiwan Ocean University, Keelung 202, Taiwan*

(Received April 12, 2010)

A systematic study of a series of $Mo_{1-x}W_xS_2$ mixed-layered crystals with $0 \leq x \leq 1$ grown by the chemical vapor transport method was conducted by using Raman scattering measurements. The composition of the samples was determined by X-ray photoelectron spectroscopy. Measurements in the basal plane revealed two dominant first-order Raman-active modes A_{1g} and E^1_{2g} as well as several second-order modes in the range of 250–450 cm^{-1}. The E_{1g} mode was observed in the edge plane of thick samples. For all the $Mo_{1-x}W_xS_2$ samples, the peaks corresponding to the A_{1g} mode showed one-mode behavior, whereas the peaks corresponding to the E^1_{2g} mode exhibited two-mode behavior. These results can be explained on the basis of the atomic displacements for each mode. In the case of the A_{1g} mode, only sulfur atoms vibrate, and this results in the one-mode behavior. In contrast, in the case of the E^1_{2g} mode, metal atoms and sulfur atoms vibrate together, and the resulting mass difference between the vibrating Mo and W cations results in the two-mode behavior of the peaks corresponding to the E^1_{2g} mode.

PACS numbers: 63.20.-e; 63.22.-m; 78.20.-e; 78.30.-j

I. INTRODUCTION

Layered semiconductors with the chemical formula TX_2 (T = Mo, W; X = S, Se, Te) have a two-dimensional layered-type structure that causes most of their physical properties to be anisotropic [1–4]. Layered TX_2 materials have also been extensively investigated because of their potential practical applications, e.g., in manufacturing efficient electrodes for photoelectrochemical solar cells [5–7], for use as catalysts in industrial applications and as solid-state lubricants [11–13], and in manufacturing secondary batteries [8–10]. Over the last two decades, several papers have been published on the preparation of $Mo_{1-x}W_xS_2$ compounds directly from the constituent elements and their characterization [14, 15]; papers have also been published on nanotubes and related structures [16–18]. By performing piezoreflectance measurements in the vicinity of the direct band-edge, it has been found that the transition energies of the $Mo_{1-x}W_xS_2$ compounds [15] vary smoothly with the tungsten content x.

In this paper, we performed a systematic Raman scattering study of a series of

$Mo_{1-x}W_xS_2$ mixed-layered crystals grown by the chemical vapor transport method. X-ray photoelectron spectroscopy (XPS) was employed to determine the composition of the $Mo_{1-x}W_xS_2$ samples. The peaks corresponding to the dominant first-order Raman-active modes A_{1g} and E^1_{2g} and of several second-order modes were observed in the basal plane of the crystals. Moreover, the E_{1g} mode was observed in the edge planes of the thick MoS_2 samples. Polarization-dependent backscattering measurements were performed to accurately determine the positions of the A_{1g} and E^1_{2g} modes in the $Mo_{1-x}W_xS_2$ samples with different x. For all the sample crystals, the peaks corresponding to the A_{1g} mode showed one-mode behavior, while the peaks corresponding to the E^1_{2g} mode showed two-mode behavior. The composition-dependent behaviors of the A_{1g} and E^1_{2g} modes were discussed.

II. EXPERIMENT

Single crystals of $Mo_{1-x}W_xS_2$ solid solutions were grown by the chemical-vapor transport method [15]. Powdered compounds were prepared from the constituent elements (Mo: 99.99%; W: 99.95%; S: 99.999%) prior to crystal growth by carrying out a reaction at 1000 °C for 10 days in evacuated quartz ampoules. W and Mo were added such that x changed from 0 to 1 with a step size Δx of 0.1. The mixture was heated up to 1000 °C slowly to avoid any explosions that could occur as a result of the strongly exothermic reaction between the elements. Chemical transport was achieved with Br_2 as the transport agent; approximately 8 mg/cm^3 of Br_2 was used. The growth temperature was set at 1030 → 980 °C with a temperature gradient of 3 °C/cm and a growth time of 20 days. The crystals had the shape of thin-layered plates with thicknesses and surface areas ranging from 20 to 1000 μm and 20 to 100 mm^2, respectively. X-ray analysis confirmed that the samples were single-phase materials with a 2H-type structure for all values of x.

XPS measurements were carried out using a Thermo VG Scientific Theta Probe system and an achromatic Al Kα line (1486.68 eV) X-ray source operated at 15 kV and with an emission current of 7 mA. The spectrometer was calibrated by the photoemission line of Ag $3d_{5/2}$ at 368.28 eV. The sample surfaces were cleaned under vacuum by argon ion etching until reproducible spectra were obtained. The base pressure of the vacuum chamber was 10^{-9} Torr. Using the Thermo VG Scientific Theta Probe system, accurate peak positions of the binding energies of the $Mo_{1-x}W_xS_2$ solid solutions were determined; this was achieved by curve fitting using a mixture of Gaussian and Lorentzian line shapes after treatment of the background by a Shirley function. Figures 1(a)–(c) show the slow-scan XPS spectra in the vicinity of the W 4f, S 2p, and Mo 3d signals of the $Mo_{1-x}W_xS_2$ single crystals, respectively. The line shapes corresponding to the main photoelectron peaks (W $4f_{7/2,5/2}$, S $2p_{3/2,1/2}$, and Mo $3d_{5/2,3/2}$) in the case of $Mo_{1-x}W_xS_2$ show no obvious differences. The ratio of the intensity of W $4f_{7/2}$ to that of W $4f_{5/2}$ (Fig. 1(a)) and the ratio of the intensity of Mo $3d_{5/2}$ to that of Mo $3d_{3/2}$ (Fig. 1(c)) are consistent with the theoretical value of 4:3 and 3:2, respectively,, while the ratio of the intensity of S $2p_{3/2}$ to that of S $2p_{1/2}$ (Fig. 1(b)) correspond to the theoretical value of 2:1; this suggests that the

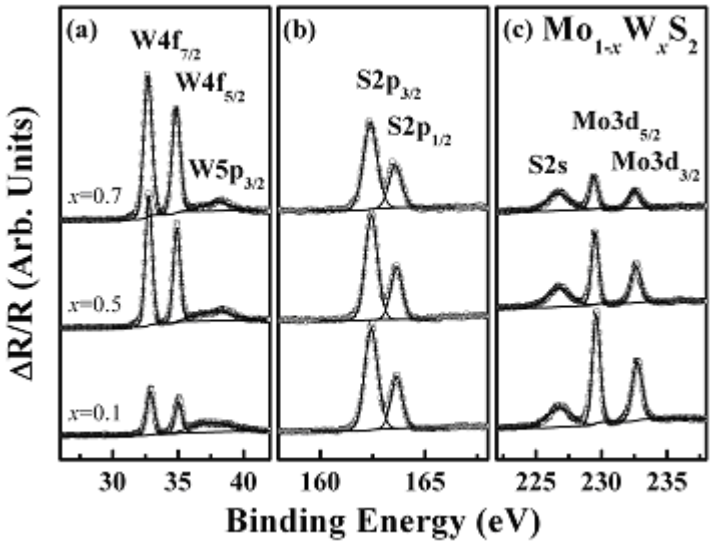

FIG. 1: The XPS spectra in the vicinity of the (a) W 4f, (b) S 2p, and (c) Mo3 3d peaks Mo_{1-x} W_x S_2 single crystals at $x = 0.1, 0.5$, and 0.7.

as-grown $Mo_{1-x}W_xS_2$ crystals are metal disulfides. The calculated ratios of the intensity of W $4f_{7/2,5/2}$ to that of Mo $3d_{5/2,3/2}$ obtained from the XPS core-level spectra by applying a standard sensitivity-factor correction correspond quite well to the stoichiometry of the constituent element W and Mo.

Raman measurements were performed at room temperature utilizing the back-scattering configuration on a Renishaw inVia micro-Raman system with an 1800 grooves/mm grating and an optical microscope with a 50× objective. A linearly polarized Ar^+ laser beam of the 514.5 nm excitation line and with a power of $\sim$ 1.5 mW was focused on a spot with the size of $\sim$ 5 μm in diameter. Prior to the measurement, the system was calibrated by using the 520 cm^{-1} Raman peak of polycrystalline Si.

III. RESULTS AND DISCUSSION

Raman spectra of bulk 2H-TS_2 (T = Mo or W) have been studied extensively both experimentally and theoretically [19–22]. 2H-TS_2 belongs to the D^4_{6h} space group that has 12 modes of lattice vibrations at the Γ point in the hexagonal Brillouin zone [19, 21]. There are four first-order Raman-active modes in 2H-TS_2: E_{1g} (286 cm^{-1} and 306 cm^{-1}), E^1_{2g} (383 cm^{-1} and 356 cm^{-1}), A_{1g} (408 cm^{-1} and 421 cm^{-1}), and E^2_{2g} (32 cm^{-1} and 27 cm^{-1}) [20, 22]. The Raman-polarization-dependent tensors are of the form [23]:

$$\alpha(A_{1g}) = \begin{bmatrix} a & 0 & 0 \\ 0 & a & 0 \\ 0 & 0 & b \end{bmatrix},$$

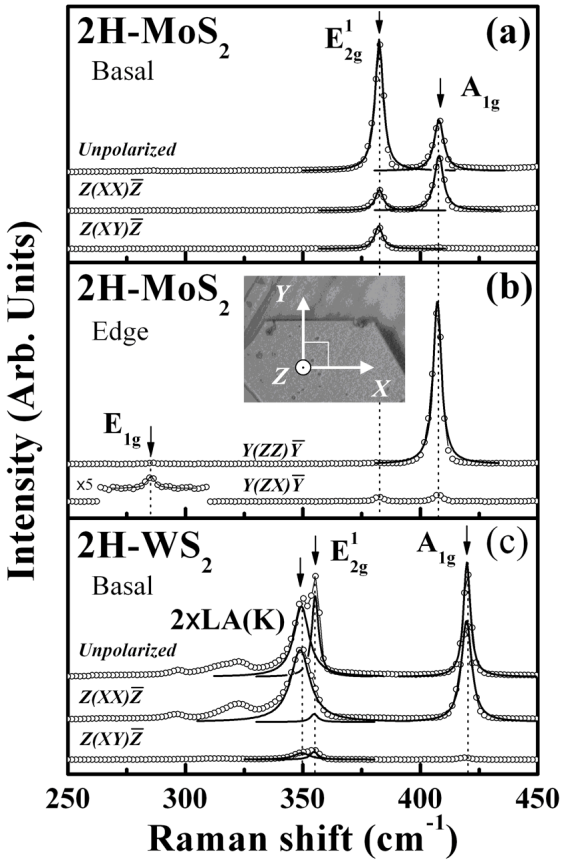

FIG. 2: Raman spectra of 2H-MoS $_2$ in the basal plane (a) and edge plane (b) as well the basal plane spectra of 2H-WS $_2$ samples (c) in the range 250–450 cm $^{-1}$. The prominent main modes A $_{1g}$ and E $^1_{2g}$ in the basal plane as well as the E $_{1g}$ mode in the edge plane measurements are seen. The solid curves are obtained by using a mixture of Gaussian and Lorentzian line shapes.

$$\alpha(E_{1g}) = \begin{bmatrix} 0 & 0 & 0 \\ 0 & 0 & c \\ 0 & c & 0 \end{bmatrix}, \qquad \begin{bmatrix} 0 & 0 & -c \\ 0 & 0 & 0 \\ -c & 0 & 0 \end{bmatrix},$$

$$\alpha(E_{2g}) = \begin{bmatrix} 0 & d & 0 \\ d & 0 & 0 \\ 0 & 0 & 0 \end{bmatrix}, \qquad \begin{bmatrix} d & 0 & 0 \\ 0 & -d & 0 \\ 0 & 0 & 0 \end{bmatrix}. \tag{1}$$

In the backscattering experiments in a basal plane, i.e., the plane perpendicular to the c-axis, the E_{1g} mode is forbidden, whereas the A_{1g} and E_{2g} modes are allowed [19, 21]. The E^2_{2g} mode, the so-called "rigid-layer" mode, is expected in the region with very low wave number [21, 24].

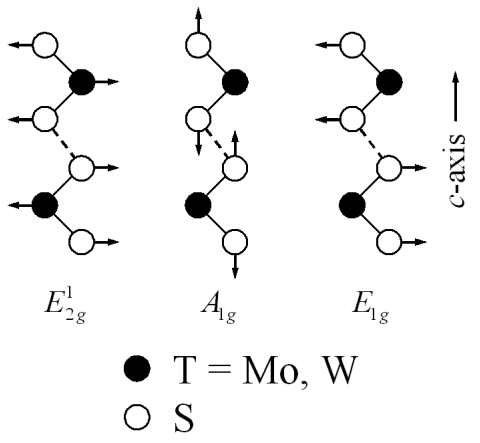

FIG. 3: Atomic-displacement vectors of six atoms in the unit cell of the polytype TS_2 layered crystals with 2H structures in the case of the Raman-active modes A_{1g} and E^1_{2g}, observed in the basal plane as well as in the case of the E_{1g} mode observed in the edge plane.

To accurately determine the positions of the E_{1g}, E^1_{2g}, and A_{1g} modes as well as the second-order Raman (SOR) features in the vicinity of the E^1_{2g}, polarization-dependent backscattering measurements have been carried out. The widely used Porto notation [25] has been utilized in this study for the designation of the crystal and polarization directions. The [100], [010], and [001] crystallographic axes are denoted by the letters X, Y, and Z (see the inset of Fig. 2), respectively. In the basal plane measurements, the notation $Z(XX)\overline{Z}$ indicates that the direction of incident radiation is along Z; the first and second letters in the bracket denote the polarization of the incident and scattered light, respectively, and $\overline{Z}$ represents the direction of the scattered light, which is opposite to Z. For the $Z(XX)\overline{Z}$ configuration, the analyzer is placed just in front of the charge coupled device (CCD) camera such that its polarization axis is parallel to the polarization axis of the incident linearly polarized laser beam. A fine adjustment in the orientation of the [100] crystallographic axis of the sample to coincide with the **E** vector of the incident linearly polarized laser beam is achieved by maximizing the intensity of the A_{1g} mode. The $Z(XY)\overline{Z}$ configuration is obtained by simply placing the half-wavelength plate directly between the analyzer and CCD. For the edge plane, $Y(ZZ)\overline{Y}$ and $Y(ZX)\overline{Y}$ polarization configuration measurements are also performed.

Figure 2 depicts the polarization-dependent Raman spectra of 2H-MoS_2 measured in the basal plane (Fig. 2(a)) and the edge plane (Fig. 2(b)) as well as the basal plane spectra of 2H-WS_2 samples (Fig. 2(c)) in the range 250–450 cm^{-1}. The spectra reveal the first-order Raman signals as well as the SOR processes that are a result of the coupling of phonons with non-zero momenta. Two prominent first-order Raman-active modes E^1_{2g} and A_{1g} for 2H-TS_2 single crystals exhibit pronounced polarization dependence of the $Z(XX)\overline{Z}$ and $Z(XY)\overline{Z}$ configurations. These modes result from the vibration of atoms within an S-T-S layer (see Fig. 3). In the case of 2H-WS_2 (Fig. 2(c)), we can observe a splitting of

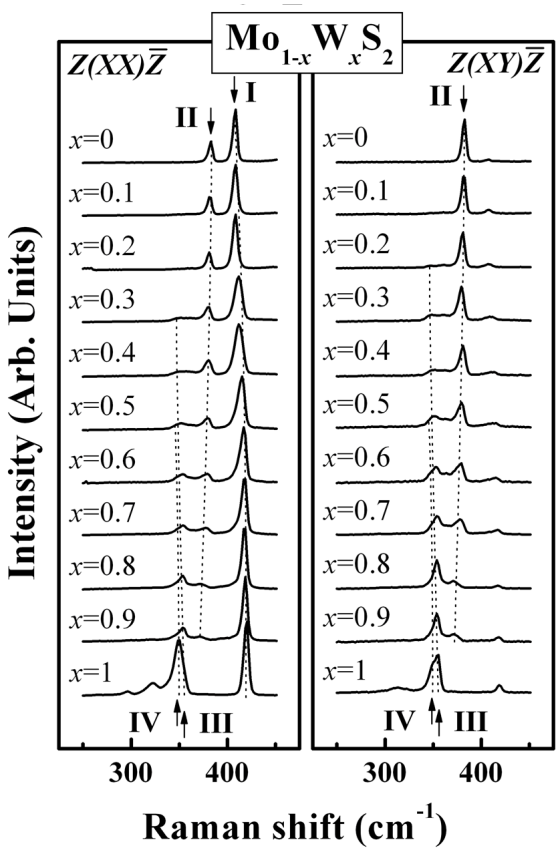

FIG. 4: Polarized Raman spectra of Mo_{1-x} W_x S_2 mixed-layered crystals in the range 250–450 cm^{-1} with the $Z(XX)\overline{Z}$ and $Z(XY)\overline{Z}$ configurations. The arrows show the position of the main features labeled as I, II, III, and IV.

the feature at around 355 cm^{-1} into two peaks. On the basis of previous reports [20, 22], the peaks are tentatively attributed to the first-order E^1_{2g} mode and to a feature attributed to the SOR band associated with the 2LA(K) overtone.. The other SOR features can be attributed to combinations of bands involving phonons at the K point coupled to the LA(K) mode [26]. The results obtained in the edge plane ($Y(ZZ)\overline{Y}$ and $Y(ZX)\overline{Y}$ configurations) measurements (Fig. 2(b)) show the polarization-dependent behavior of the A_{1g} and E_{1g} modes for 2H-MoS_2. In the case of the $Y(ZZ)\overline{Y}$ configuration, the A_{1g} mode is dominant, whereas the mode almost disappears in the case of the $Z(XY)\overline{Z}$ measurements. The peak corresponding to the E_{1g} mode is absent in the case of the $Y(ZZ)\overline{Y}$ configuration, and it can be observed only in the case of the $Z(XY)\overline{Z}$ polarization configuration. The energies and relative intensities of the features observed in the basal and edge plane for both 2H-MoS_2 and 2H-WS_2 spectra correspond well to the previously reported Raman lines [19–22].

The polarization-dependent Raman spectra measured in the basal plane of several $Mo_{1-x}W_xS_2$ mixed-layered crystals for wave numbers in the range 250–450 cm^{-1} are shown

in Fig. 4. From top to bottom, x increases from 0 to 1 with a composition step size Δx of 0.1; the increase corresponds to the stoichiometry of the constituent elements W and Mo. The polarization-dependent Raman spectra of the binary MoS_2 and WS_2 layered compounds have been discussed previously and are included in Fig. 4 for the purpose of comparison. By comparing the polarization dependence and position dependence of the observed features in the case of the mixed ternary compound with those of the binary end compounds, we can determine whether the feature corresponds to the A_{1g} mode, MoS_2-like E^1_{2g} mode, WS_2-like E^1_{2g} mode, or the SOR band due to 2LA(K) overtone.

With an increase in x, feature I shifts to a higher wave number. In contrast, as x increases, feature II shifts to a lower wave number with a decrease in its peak intensity. Further, with an increase in x, two additional features III and IV appear in the lower-wave-number region of the Raman spectra of the $Mo_{1-x}W_xS_2$ samples. These two features can be accurately identified from their polarization dependence; while feature III is dominant in the case of $Z(XY)\overline{Z}$ polarization, feature IV is dominant in the case of $Z(XX)\overline{Z}$ polarization. Both features show a blue shift and become the dominant features at higher x values. Hence, as can be seen from Fig. 4, feature I corresponding to the A_{1g} mode exhibits a one-mode behavior, whereas features II and III corresponding to the E^1_{2g} mode exhibit a two-mode behavior. Feature IV is identified to be the SOR band due to 2LA(K) overtone. Furthermore, features II and III are designated as MoS_2-like E^1_{2g} and WS_2-like E^1_{2g} modes, respectively, on the basis of the shift in their position with x. These experimental results can be explained satisfactorily on the basis of the atomic displacements for each mode. In the case of the A_{1g} mode, only sulfur atoms vibrate and this give rise to the one-mode behavior of the mixed-layered crystals. On the other hand, in the case of the E^1_{2g} mode, metal atoms and sulfur atoms vibrate together (see Fig. 3). The atomic weight of tungsten is 1.92 times greater than that of molybdenum, and this mass difference results in the two-mode behavior of the E^1_{2g} mode. These composition-dependent behaviors are often seen in the Raman spectra of solid solutions in which there is no ordered distribution of the constituent atoms [27, 28].

IV. SUMMARY

The Raman spectra of $Mo_{1-x}W_xS_2$ mixed-layered crystals over a wide range of compositions ($0 \leq x \leq 1$) were investigated. In the range of 250–450 cm^{-1}, the first-order Raman-active modes A_{1g} and E^1_{2g} were observed in the basal plane of the layered crystals, while the E_{1g} mode was observed in the edge plane for the thick samples. For the entire $Mo_{1-x}W_xS_2$ series, the peaks corresponding to the A_{1g} mode show one-mode behavior, while the peaks corresponding to the E^1_{2g} mode exhibit two-mode behavior. These results are explained on the basis of the atomic displacements in the case of each mode. In the case of the A_{1g} mode, only sulfur atoms vibrate, and this results in the one-mode behavior of the mixed-layered crystals. On the other hand, in the case of the E^1_{2g} mode, the metal atoms and the sulfur atoms vibrate together, and the mass difference between the vibrating Mo and W cations results in the two-mode behavior of the E^1_{2g} mode.

Acknowledgments

The authors would like to acknowledge the financial support provided by the National Science Council of Taiwan through Grant Nos. NSC 97-2112-M-011-001-MY3 and NSC 98-2811-M-011-003.

References

* Electronic address: ysh@mail.ntust.edu.tw

[1] J. A. Wilson and A. D. Yoffe, Adv. Phys. **18** 193 (1969).
[2] A. R. Beal, J. C. Knights, and W. Y. Liang, J. Phys.: Solid State Phys. **5** 3540 (1972).
[3] L. F. Mattheiss, Phys. Rev. B **8** 3719 (1973).
[4] E. Fortin and F. Raga, Phys. Rev. B **11** 905 (1975).
[5] W. Kautek, H. Gerisch, and H. Tributsch, J. Electrochem. Soc. **127** 2471 (1980).
[6] K. K. Kam and B. A. Parkinson, J. Phys. Chem. **86** 463 (1982).
[7] S. J. Li, J. C. Bernède, J. Pouzet, and M. Jamali, J. Phys.: Condens. Matter **8** 2291 (1996).
[8] P. Grange and B. Delmon, J. Less-Common Met. **36** 353 (1974).
[9] P. G. Moses, B. Hinnemann, H. Topsøe, and J. K. Nørskov, J. Catal. **248** 188 (2007).
[10] C. T. Tye and K. J. Smith, Catal. Today **116** 461 (2006).
[11] J. M. Martin, C. Donnet, Th. Le Mogne, and Th. Epicier, Phys. Rev. B **48** 10583 (1993).
[12] S. D. Walck, J. S. Zabinski, N. T. McDevitt, and J. E. Bultman, Thin Solid Films **305** 130 (1997).
[13] L. Rapoport, V. Leshchinsky, I. Lapsker, Yu. Volovik, O. Nepomnyashchy, M. Lvovsky, R. Popovitz-Biro, Y. Feldman, and R. Tenne, Wear **255** 785 (2003).
[14] S. K. Srivastava, T. K. Mandal, and B. K. Samantaray, Synthetic Metals **90** 135 (1997).
[15] C. H. Ho, C. S. Wu, Y. S. Huang, P. C. Liao, and K. K. Tiong, J. Phys.: Condens. Matter **10** 9317 (1998).
[16] C. Thomazeau, C. Geantet, M. Lacroix, V. Harlé, S. Benazeth, C. Marhic, and M. Danot, J. Solid State Chem. **160** 147 (2001).
[17] C. Thomazeau, C. Geantet, M. Lacroix, M. Danot, V. Harlé, and P. Raybaud, Appl. Catal. A: General **322** 92 (2007).
[18] M. Nath, K. Mukhopadhyay, and C. N. R. Rao, Chem. Phys. Lett. **352** 163 (2002).
[19] T. J. Wieting and J. L. Verble, Phys. Rev. B **3** 4286 (1971).
[20] J. M. Chen and C. S. Wang, Solid State Commun. **14** 857 (1974).
[21] T. Sekine, T. Nakashizu, K. Toyoda, K. Uchinokura, and E. Matsuura, Solid State Commun. **35** 371 (1980).
[22] C. Sourisseau, M. Fouassier, M. Alba, A. Ghorayeb, and O. Gorohov, Mat. Sci. Eng. B **3** 119 (1989).
[23] R. Loudon, Adv. Phys. **13** (1964).
[24] J. L. Verble, T. J. Wieting, and P. R. Reed, Solid State Commun. **11** 941 (1972).
[25] T. C. Damen, S. P. S. Porto, and B. Tell, Phys. Rev. **142** 570 (1966).
[26] C. Sourisseau, F. Cruege, M. Fouassier, and M. Alba, Chem. Phys. **150** 281 (1991).
[27] M. Ishii and M. Saeki, Solid State Commun. **67** 895 (1988).
[28] I. F. Chang and S. S. Mitra, Adv. Phys. **20** 359 (1971).